DOI: ADD DOINUMBER HERE

Numerical Configuration Study of Ionic Wind for Propulsion via a Two-Way Electro-Aero-Dynamic Modelling

J. M. D.C. Marques⋆*, D. Fabre*⋆ *and F.Plouraboué*⋆
⋆*Institut de Mé canique des Fluides, IMFT, Université de Toulouse, CNRS, Toulouse, France*
fplourab@imft.fr

Abstract

This contribution is interested in the modelling of ionic wind generated by a stationary corona discharge within a steady imposed external flow. When considering an adverse fluid velocity larger than ten meter per second, the usually used one way coupling approximation falls short and a two-way coupling arises between charges drift and fluid flow. This contribution uses an asymptotic two-way coupling over a multi-scaled two-domain approach based upon a non-dimensional number M_c being the ratio between the external velocity flow to the drift charges one, to evaluate the propulsive properties of a one emitter two NACA0012 collector system.

1. Introduction

Electro-Aero-Dynamic (EAD) low-plasma gas flows are of interest in many applications such as particles cleaning with electro precipitators[2,1] electronic cooling, flame ignition control, plane safety against storms. In the last couple of years this technology has resurfaced as it provides a near-silent, electric and without moving parts alternative to in-atmosphere propulsion,[13,22,21]

EAD flows are usually generated by direct current corona discharges (CD), as creating CD are well a known and relatively easy way to generate ionic wind.[19] These were studied in the sixties in the context of plane safety against storms by S.Chapman[3] and later by Guerra-Garcia et al.[9] They performed wind tunnel experiments for various electrode configurations and measured the influence of a high velocity external flow, up to 200 m/s on the current-voltage characteristic, both finding currents linear variation with the imposed external velocity. This finding has recently been confirmed by Grosse et al.[8] at lower velocities.

Even though corona discharge or ion drift numerical modelling has already been successfully accomplished by several authors,[14,1,23,45]), to the best of our knowledge, it wasn't until very recently that the coupling of an external flow with charge drift in a CD was successfully numerically modelled. Usually a so called "one-way approximation" is used, it consists of noting that the electrical charge transport problem producing the current is decoupled from the fluid flow. This approximations is only valid when the adverse fluid velocity is of the order of 10 m/s, whereby the fluid advection influence is neglected. This approximation results in a one-way coupling of the charges onto the flow. A recent numerical and experimental study by Picella et al.[17] has considered the one-way coupling and accurately compared it with experiments, in the framework of the Kaptzov hypothesis, which is a simplified approach to model CD, only asymptotically valid.[16]

In works under review, it was shown that the two-way coupling could be achieved via an asymptotic expansion based upon a non-dimensional number M_c being the ratio between the external velocity flow to the drift charges one. That one-way approximation acts as a leading order problem to the CD in the presence of an external flow and the retroactive action of the fluid advection into the charge drift, to which the retroactive effect acts as a first order correction. This approach method was successfully compared to recent experimental results[89] so as to validate the numerical model.

In this contribution we propose to use this new two-way asymptotic formulation of the EAD low-plasma gaz flows to study the propulsive properties of a one emitter two NACA0012 collector system.

In section 2 the dimensionless models and asymptotic expansion according to the dimensionless number M_c are recalled. This expansion permits to find a simplified iterative two-way formulation composed of a dominant problem corresponding to the previously mentioned one-way model,[917] and a first order problem being the linearised base problem coupled with the linearised dominant base problem. In section 3, the numerical model will be applied to the one emitter two NACA0012 collector configuration to study the effect of the external flow on the propulsive capabilities of this system by changing the emitter-collector distance as well as the inter-collector distance at a constant external

electric field. To determine the optimal geometries, the relevant reference quantities i.e. EAD thrust and thrust density, thrust-to-power and kinetic efficiency will be compared.

2. Methods

2.1 Dimensionless Governing Equations

Let us define the dimensionless formulation, by setting the reference quantities. This exactly the same as Monrolin et al.([16] and[14]) and Picella et al.[17] and even[6] have done with the addition of the advection of charged species that will be responsible for the previously mentioned two-way coupling. Starting off by setting the reference dimensionless quantities φ_a is the applied potential at the emitter, r_c the reference length as the NACA0012 collector maximum thickness and n_k^* the reference charge number density, which is defined identically to Monrolin et al.,[12]

$$n_k^* = \frac{\varepsilon_0 \varphi_a}{e r_c^2} \frac{\mu_p}{\mu_k}$$

where $k = e,\ p,\ n$, for electrons, positive and negative ions. In the case of the fluid variables, the reference speed of the ionic wind velocity is set

$$U_e = \sqrt{\frac{\varepsilon_0}{\rho_f}} \frac{\varphi_a}{r_c} \tag{1}$$

and reference pressure

$$p^* = \rho_0 U_e^2$$

.
Then, just line in Monrolin et al.,[15] a small asymptotic parameter ε is defined allowing to compare the applied field to the "internal" field defined by the ionization electric field in the Townsend law :

$$\varepsilon = \frac{\varphi_a}{L E_i} \tag{2}$$

ε justifies in Monrolin et al.,[14] an asymptotic expansion, separating the domain into two distinct domains, each with its own modelling.
For reference the dimensionless parameters are :

$$\varphi = \frac{\varphi^*}{\varphi_a},\ \mathbf{r} = \frac{\mathbf{r}^*}{r_c},\ \mathbf{u} = \frac{\mathbf{u}^*}{U_e},\ p = \frac{p^*}{\rho_f U_e^2},\ n_k = \frac{n_k^*}{\frac{\varepsilon_0 \varphi_a}{e r_c^2} \frac{\mu_p}{\mu_k}}, \tag{3}$$

Using these reference dimensionless parameters we obtain the following dimensionless formulation of the system (**??**).

$$\begin{cases} \Delta\varphi = -\dfrac{e}{\varepsilon_0}(n_p - n_n - \delta_\mu n_e) \\ \nabla \cdot [n_e(-\delta_\mu \nabla\varphi + M_c \mathbf{u}) - \dfrac{1}{P_e}\nabla n_e] = (\alpha - \eta)\|\mathbf{j_e}\| + \gamma S \\ \nabla \cdot [n_p(-\nabla\varphi + M_c \mathbf{u}) - \dfrac{1}{P_e}\nabla n_p] = \alpha\|\mathbf{j_e}\| + \gamma S \\ \nabla \cdot [n_n(-\nabla\varphi + M_c \mathbf{u}) - \dfrac{1}{P_e}\nabla n_n] = \eta\|\mathbf{j_e}\| \\ \mathbf{u} \cdot \nabla\mathbf{u} + \nabla p - \dfrac{1}{R_e}\Delta\mathbf{u} = -(n_p - n_e - n_n)\nabla\varphi \\ \nabla \cdot \mathbf{u} = 0 \end{cases} \tag{4}$$

Where appears an electric Mach, which is the ratio between the electric macroscopic and microscopic speeds number, of the order of 10^{-2} :

$$M_c = \frac{1}{\mu_p}\sqrt{\frac{\varepsilon_0}{\rho_f^*}} \tag{5}$$

then, an electrical Peclet number of the order 10^4 :

$$P_e = \frac{\mu_p \varphi_a}{D_\rho} \tag{6}$$

and and the ration between ion and electron mobilities also of the order of 10^{-2}: $\delta_\mu = \frac{\mu_p}{\mu_e}$

Next dimensionless border conditions are expressed, they are no different from Monrolin et al.'s.[14]

- The electric potential fulfils a global elliptic problem with Dirichlet boundary conditions, on each electrode :

$$\varphi_{|\partial\Omega_e} = 1 \quad \& \quad \varphi_{|\partial\Omega_c} = 0 \tag{7}$$

- There are no electron fluxes on the collecting electrode and no ion fluxes on the emitting electrode :

$$\mathbf{j}_p \cdot \mathbf{n}_{|\partial\Omega_e} = 0 \quad \& \quad \mathbf{j}_e \cdot \mathbf{n}_{|\partial\Omega_c} = 0 \tag{8}$$

- The flux of ion charge and normal electric field are imposed null at the outer boundaries of the domain :

$$\mathbf{E} \cdot \mathbf{n}_{|\partial\Omega_{in} \cup \partial\Omega_{out} \cup \partial\Omega_{top} \cup \partial\Omega_{bot}} = 0 \quad \& \quad \mathbf{j}_p \cdot \mathbf{n}_{|\partial\Omega_{in} \cup \partial\Omega_{out} \cup \partial\Omega_{top} \cup \partial\Omega_{bot}} = 0 \tag{9}$$

- No-slip velocity at the emitter and collector surfaces for the fluid boundary conditions :

$$\mathbf{u}_{|\partial\Omega_e} = \mathbf{0} \quad \& \quad \mathbf{u}_{|\partial\Omega_c} = \mathbf{0} \tag{10}$$

As well as a stress-free velocity condition over the downstream and lateral boundaries:

$$\sigma \cdot \mathbf{n}_{|\partial\Omega_{top} \cup \partial\Omega_{bot} \cup \partial\Omega_{out}} = \mathbf{0} \tag{11}$$

where σ is the dimensionless stress-tensor. Lately, a constant velocity is imposed U_{in} for the inlet boundary and tangential stress-free condition :

$$\mathbf{u} \cdot \mathbf{n}_{|\partial\Omega_{in}} = \frac{U_{in}}{U_e} \quad \& \quad \mathbf{t} \cdot \sigma \cdot \mathbf{n}_{|\partial\Omega_{in}} = 0 \tag{12}$$

2.2 Linear Expansion in M_c

A linear first order expansion with regards to the M_c parameter is done. Note that this expansion seems to be verified experimentally for the current intensity for air flows of up to 50 m/s by Grosse et al.,[8] Guerra-Garcia et al.[9] and even up to higher speeds by Chapman.[3]
From this expansion can be derived two different problems, one at the leading order and another at the 1st order.

This system is a "one-way" coupled problem, i.e. the electrical problem does not depend on the fluid problem, but the fluid problem is coupled with the electrical problem through the Coulomb forcing. The two-way coupling involves a feed-back of the fluid velocity within the ion drift flux conservation, which arises from the first order expansion, which corresponds to the linearised version of previous system of equations with source term for the charge conservation equations coming from the leading order charge advection, we are respectively referring to the terms : $-\nabla \cdot (n_e^0 \mathbf{u}^\mathbf{0})$, $-\nabla \cdot (n_p^0 \mathbf{u}^\mathbf{0})$, $-\nabla \cdot (n_n^0 \mathbf{u}^\mathbf{0})$.

So that the previous system is also a one-way problem, who differs from the leading order one by being linear and having a source term that comes from the leading order charge advection, that ensure the feed-back of the fluid velocity within the ion drift flux conservation.

2.3 Multi-scale two-domain modeling of the positive DC corona discharge

As the leading order electrostatic problem is exactly the same as Monrolin et al's,[14] the same numerical approach to solve the two-way problem is used, that means using a multi-scale two-domain model of the DC corona discharge, separating the computational domain into two regions : inner ionisation one and an outer drift one.
Physical mechanisms at play in the inner and outer domain are very distinct from one another, so that they can be modelled separately communicating via appropriate matching conditions at the border of the two regions.
The asymptotic expansion from Monrolin et al.'s expansion follows the previously defined parameter ε.

2.4 Numerical Methods

Numerical schemes were based on the Finite Element Methods (FEM), implemented with the finite element software FreeFem++.[?] Monitoring and post-processing was done with the Stabfem interface,[7] taking advantage of the anterior works of Monrolin et al.[14] and Picella et al.[17] .
We will not detail the numerical implementation any of the systems arising from the linear expansion in (**??**) as they use the similar stabilized methods as those described in previously referenced articles, with the exception that Navier-Stokes equations were also implemented using a SUPG-stabilized[1018] variational formulation.
The method successfully retrieves the linear trend of current intensity (18) and EHD thrust (19) with external flow, this can be justified even at high speeds as the parameter M_c 5 depends solely on atmospheric characteristics, so to attain high speeds it is sufficient to run a few low speed and extrapolate up to high speeds. This methods has been experimentally validated against experimental results from Grosse et al.[8] and Guerra-Garcia et al.[9] in works under review.

3. Parametric study of the two NACA0012 collector configuration

3.1 Description of the configuration

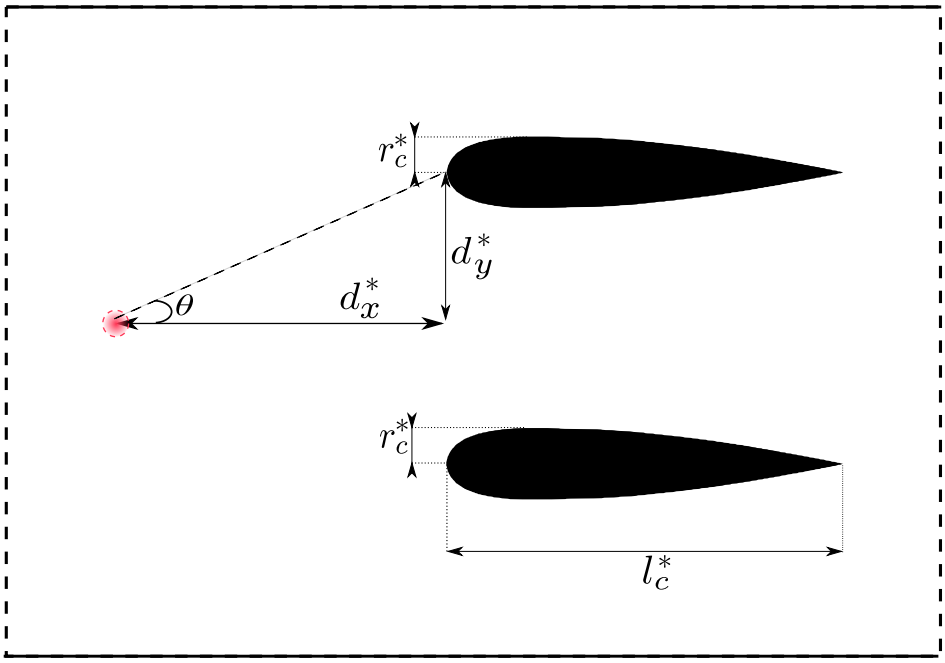

Figure 1: Studied Configuration

This section aims to study the emitter to two NACA0012 collector configuration, depicted in fig. 1 by varying the emitter-collector distance d_x^* and the inter-collector distance d_y^* whilst maintaining a constant electric field at $E_{ext} = \varphi_a / \sqrt{d_x^2 + d_y^2} = 5\text{kV/cm}$. This is equivalent to changing the angle between the emitter-to-collector and the horizontal plane noted θ. The chord has a constant length of $l_c = 5\ cm$ and a constant maximum thickness of $2r_c = 6\ mm$ and the radius of the emitter is of $50\ \mu m$

3.2 Important quantities

So as to determine the optimal configuration for this specific geometry, the reference quantities are :

- Current intensity :

$$I^* = \int_{\partial\Omega_c} \mu n_p^\star \frac{\varphi_a}{r_c} (n_p^0 E^0 \ + \ M_c (n_p^0 E^1 \ + \ n_p^1 E^0) \ ) \tag{13}$$

- EHD Thrust :

$$T^* = \int_{\Omega} n_p^{*0} E^{*0} \ + \ M_c (n_p^{*0} E^{*1} \ + \ n_p^{*1} E^{*0}) \tag{14}$$

- EHD Thrsut density :

$$\Phi^* = \frac{T^*}{2d_x} \tag{15}$$

- Thrust-to-Power ratio :

$$T^*/P^* = \frac{T}{I \cdot V} \tag{16}$$

- Kinetic efficiency :

$$\eta^* = \frac{\int_\Omega n_p^* \mathbf{E}^* \cdot \mathbf{u}^*}{\int_\Omega n_p^* \mathbf{E}^* \cdot (\mathbf{u}^* + \mu \mathbf{E}^*)} \tag{17}$$

Let us also recall the following important relationships of current intensity and thrust in the absence of an external flow :

$$I = \frac{K(\varphi_a - \varphi_{ign})\varphi_a}{d_x^2} \tag{18}$$

$$T = \frac{I * d}{\mu} = \frac{K(\varphi_a - \varphi_{ign})\varphi_a}{\mu d_x} \tag{19}$$

$$\Phi = \frac{T}{2d_x} = \frac{K(\varphi_a - \varphi_{ign})\varphi_a}{2\mu d_x^2} \tag{20}$$

Where φ_{ign} is the ignition voltage of the discharge and K is a constant dependant on the geometry of the system. These equations are useful for better understanding the numerical results.

3.3 Variation of the electrode distance d_x and d_y

Tables 1 and 2 summarize the ways in which we vary d_x and d_y and φ_a so as to study the variation of angle θ whilst maintaining a constant external electric field of E_{ext} = 5 kV/cm. In this section, the propulsive characteristics of the different configurations of each angle will be analysed both in order of magnitude and trend, so as to observe the robustness of the angle and the determine the optimal configuration.

Table 1: Different characteristic values for the geometry varying d_x

θ [°]	15	30	45	60
φ_a [V]	20705	23094	28284	40000
d_y [cm]	1.1	2.3	4	6.9
d_x = 4 cm				

Table 2: Different characteristic values for the geometry varying d_x

θ [°]	15	30	45	60
φ_a [V]	77247	40000	28284	23094
d_x [cm]	14.9	6.9	4	2.3
d_y = 4 cm				

Figure 2's left panel compares generated EHD Thrust for different values of the angle θ obtained by varying d_y (cf. table 1, dashed lines) and d_x (cf. table 2, continuous lines), and the right panel shows a comparison of generated EHD Thrust density for different values of the angle θ obtained by varying d_y (cf. table 1) represented by the dashed lines and d_x (cf. table 2) represented by the continuous lines. The star dots represent the results of the simulations

which were extrapolated so as to reach 75 m/s. Varying the d_x length generates a better net EHD thrust, this is not surprising as for a same value of θ, varying d_x applies a higher potential and a larger emitter-collector distance, which even in the absence of an external flow is prone to generating higher values of thrust. The bottom figure compares the generated EHD thrust density of both configurations varying d_y and d_x for various angles θ. Contrary to the thrust, the generated thrust density is of the same order of magnitude for each angle, although the trends are preserved with the external flow speed increase. This is in agreement with the fact that when we vary d_y we change the both the applied potential and surface area of the thruster, whereas when we vary d_x this does not happen, so that the generated EHD thrust is greatly amplified the smaller the surface of the thruster is. Let us also note that Wilson[20] postulated that values of EHD thrust densities equal or larger to 20 N/m^2 would be competitive with those of turbo fan engines, figure 2's last graph shows that for an angle of $\theta = 15$ °formed by adjusting d_y a quarter to half of this value can be reached.

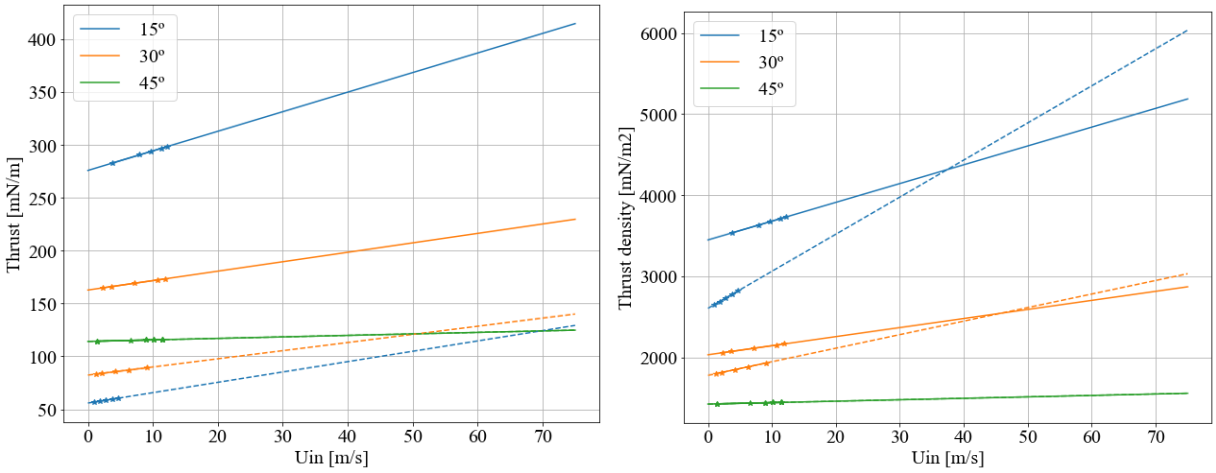

Figure 2: Left panel compares generated EHD Thrust for different values of the angleθ obtained by varying d_y (cf. table 1, dashed lines) and d_x (cf. table 2, continuous lines), and comparison of generated EHD Thrust density (right panel) for different values of the angle θ obtained by varying d_y (cf. table 1) represented by the dashed lines and d_x (cf. table 2) represented by the continuous lines. The star dots represent the results of the simulations which were extrapolated so as to reach 75 m/s.

Figure **??** compares the Thrust-to-Power ratio (on the left) and the kinetic efficiency η_K (on the right) generated when varying d_y (dashed lines) and d_x (continuous lines). In all cases, generated Thrust-to-Power seems to degradate asymptotically with external flow speed. Two main facts should be noted : firstly all cases are above the 2 N/kW limit established by Barrett[11] for competitive performances against turbofans, sometimes up to five times at no external flow speed and two and a half times asymptotically at high external flow speed. Secondly, the smaller the θ angle, the better the thrust-to-power ratios. As for the kinetic efficiency (right figure), although it increases with external flow speed, it remains small,never being larger that 10%. Here again smaller angles seem to have high efficiencies although the difference is hardly noticeable. Note that at high speeds (not represented here) efficiency seems to have the shape of an inverted power reaching around 12%.

Comparison of slopes of the generated EHD Thrust (top left), Thrust Density (top right) and Current Intensity (bottom) with external flow speed as a function of the angle θ are made in figure , these are obtained by varying d_x (cf. table 1) represented by the dashed lines and d_x (cf. table 2) represented by the continuous lines. Both top panels show that the smaller the angle the better for propulsion generation, however it is interesting to notice that the net EHD thrust generated is higher when varying the d_x length, that is the inter-electrode distance, whereas the EHD thrust density is higher when varying the d_y distance. This is related to the variation of thruster surface when varying the d_y which greatly increases the thrust density slope as it decreases. Indeed, it is worthy to note that at $\theta = 15°$ varying the d_y provides a slope about two times larger than that obtained by varying the d_x length. Finally note that there is no visible optimum for quantities, meaning that the smaller the angle the better for the propulsion generation increase with external flow speed. This is curiously not the case for the current intensity with external flow speed slope, in fat there does seem to be an optimum at about 50 °.

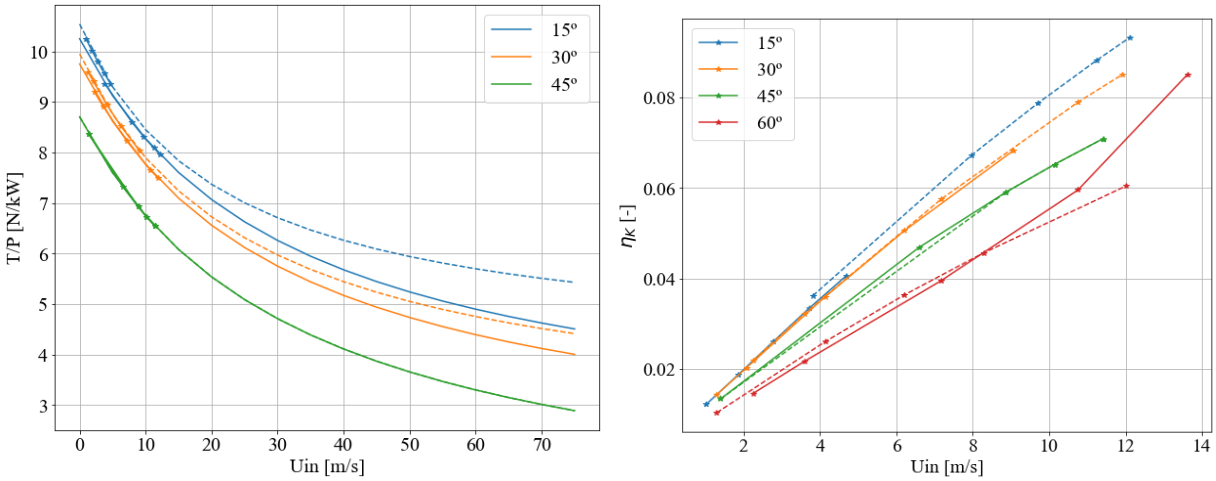

Figure 3: Comparison of generated EHD Thrust-to-Power (left) and kinetic efficiency η_K (right) with external flow speed for different values of the angle θ obtained by varying d_y (cf. table 1) represented by the dashed lines and d_x (cf. table 2) represented by the continuous lines. The star dots represent the results of the simulations which were extrapolated so as to reach 75 m/s. Note that as the kinetic efficiency η_K doesn't follow any linear trends, it cannot be extrapolated unto higher speeds.

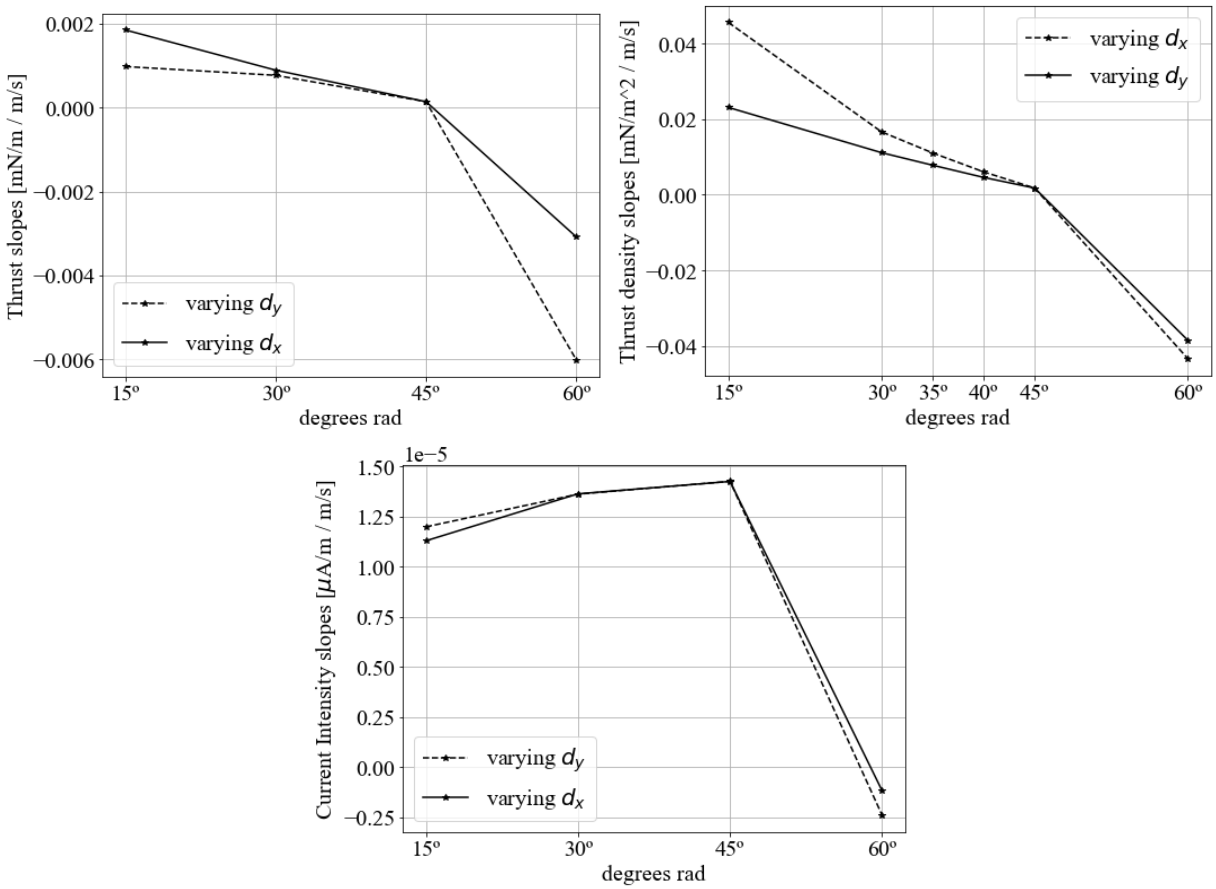

Figure 4: Comparison of slopes of the generated EHD Thrust (top left), Thrust Density (top right) and Current Intensity (bottom) as a function of the angle θ obtained by varying d_y (cf. table 1) represented by the dashed lines and d_x (cf. table 2) represented by the continuous lines.

4. Conclusion

In this paper an analysis of a steady corona discharge in the presence of an external flow within a monolithic formulation based on an asymptotic expansion has been presented. This contribution relies on a two-domains approach for

corona discharge modelling which was previously established, thus expanding the formulation the previous one-way approximation using a the described new asymptotic expansion, rendering explicit the derivation of two-way coupling between the fluid and CD to model EAD ffects. This expansion is based upon small parameter M_c : it is the ratio between macroscopic to microscopic ion velocities, recovering the (non-linear) one-way coupling approximation and providing the subsequent (linear) two-way coupling corrections to it.
Results are extrapolated to 75 m/s and a one emitter - two NACA0012 collectors configuration is studied so as to find a spacing between electrodes that is optimal for propulsion. Results show that reducing the spacing between NACA0012 collectors increases generated EHD thrust density and could be extrapolated to reach competitive values at high speed, whereas increasing the emitter-collector distance generates the most net EHD thrust, thus indicating that larger configurations with collectors closer to each other seem to be favourable for thrust generation, sometimes not straying to far away from Wilson's[20] 20 N/m^2 limit. It is also shown that with external flow speed thrust-to-power decreases asymptotically remaining larger always than the 2N/kW limit and efficiency increases with external flow speed although remaining low.
These results suggest possible perspectives for geometry optimization to find competitive configurations for thrust generation.

5. Acknowledgments

The authors wish to thank J. Sierra for several enlightening discussions as well as help in the stabilization schemes. This project has received funding from the European Union's Horizon Europe Research and Innovation Program under Grant Agreement No 101098900.

References

[1] S. Arif, D.J. Branken, R.C. Everson, H.W.J.P. Neomagus, and A. Arif. The influence of design parameters on the occurrence of shielding in multi-electrode ESPs and its effect on performance. *Journal of Electrostatics*, 93:17–30, June 2018.

[2] S. Arif, D.J. Branken, R.C. Everson, H.W.J.P. Neomagus, L.A. Le Grange, and A. Arif. CFD modeling of particle charging and collection in electrostatic precipitators. *Journal of Electrostatics*, 84:10–22, December 2016.

[3] Seville Chapman. Corona point current in wind. *Journal of Geophysical Research*, 75(12):2165–2169, April 1970.

[4] Liang Chen, Ming Dong, Ping Li, and Hakan Bagci. A hybridizable discontinuous Galerkin method for simulation of electrostatic problems with floating potential conductors. *International Journal of Numerical Modelling: Electronic Networks, Devices and Fields*, 34(6):e2804, November 2021.

[5] She Chen, Yifei Zhu, Jingyi Tu, and Feng Wang. Numerical investigation of an electroaerodynamic driven aeroplane: electrical properties, ionic wind and flight performance. *Journal of Physics D: Applied Physics*, 52(36):365203, September 2019.

[6] S. Coseru, D. Fabre, and F. PlourabouÃ©. Numerical study of ElectroAeroDynamic force and current resulting from ionic wind in emitter/collector systems. *Journal of Applied Physics*, 129(10):103304, March 2021.

[7] D. Fabre, V. Citro, D. Ferreira Sabino, P. Bonnefis, J. Sierra, F. Giannetti, and M. Pigou. A Practical Review on Linear and Nonlinear Global Approaches to Flow Instabilities. *Applied Mechanics Reviews*, 70(6):060802, November 2018.

[8] Sylvain Grosse, Nicolas Benard, and Eric Moreau. Electroaerodynamic thrusters: Influence of a freestream on the current, ionic wind, and force produced by a DC corona discharge. *Journal of Electrostatics*, 130:103950, August 2024.

[9] C. GuerraâGarcia, N. C. Nguyen, T. Mouratidis, and M. MartinezâSanchez. Corona Discharge in Wind for Electrically Isolated Electrodes. *Journal of Geophysical Research: Atmospheres*, 125(16):e2020JD032908, August 2020.

[10] Volker John. *Finite Element Methods for Incompressible Flow Problems*, volume 51 of *Springer Series in Computational Mathematics*. Springer International Publishing, Cham, 2016.

[11] Kento Masuyama and Steven R. H. Barrett. On the performance of electrohydrodynamic propulsion. *Proceedings of the Royal Society A: Mathematical, Physical and Engineering Sciences*, 469(2154):20120623, June 2013.

[12] N. Monrolin, F. PlourabouÃ©, and O. Praud. Electrohydrodynamic Thrust for In-Atmosphere Propulsion. *AIAA Journal*, 55(12):4296–4305, December 2017.

[13] Nicolas Monrolin. *Ãtude thÃ©orique et expÃ©rimentale de la propulsion Ã©lectrohydrodynamique dans l'air*. Theses, Institut National Polytechnique de Toulouse - INPT, September 2018. Issue: 2018INPT0086.

[14] Nicolas Monrolin and Franck PlourabouÃ©. Multi-scale two-domain numerical modeling of stationary positive DC corona discharge/drift-region coupling. *Journal of Computational Physics*, 443:110517, October 2021.

[15] Nicolas Monrolin, Olivier Praud, and Franck PlourabouÃ©. Electrohydrodynamic ionic wind, force field, and ionic mobility in a positive dc wire-to-cylinders corona discharge in air. *Physical Review Fluids*, 3(6):063701, June 2018.

[16] Nicolas Monrolin, Olivier Praud, and Franck PlourabouÃ©. Revisiting the positive DC corona discharge theory: Beyond Peek's and Townsend's law. *Physics of Plasmas*, 25(6):063503, June 2018.

[17] Francesco Picella, David Fabre, and Franck PlourabouÃ©. Numerical Simulations of Ionic Wind Induced by Positive DC-Corona Discharges. *AIAA Journal*, pages 1–12, April 2024.

[18] Alfio Quarteroni. *Numerical Models for Differential Problems*. Springer Milan, Milano, 2014.

[19] I. P. RaÄzer. *Gas discharge physics*. Springer.

[20] Jack Wilson, Hugh D Perkins, and William K Thompson. An investigation of ionic wind propulsion. Technical report, 2009.

[21] Haofeng Xu, Nicolas Gomez-Vega, Devansh R Agrawal, and Steven R H Barrett. Higher thrust-to-power with large electrode gap spacing electroaerodynamic devices for aircraft propulsion. *Journal of Physics D: Applied Physics*, 53(2):025202, January 2020.

[22] Haofeng Xu, Yiou He, Kieran L. Strobel, Christopher K. Gilmore, Sean P. Kelley, Cooper C. Hennick, Thomas Sebastian, Mark R. Woolston, David J. Perreault, and Steven R. H. Barrett. Flight of an aeroplane with solid-state propulsion. *Nature*, 563(7732):532–535, November 2018.

[23] K Yanallah, F Pontiga, A FernÃ¡ndez-Rueda, and A Castellanos. Experimental investigation and numerical modelling of positive corona discharge: ozone generation. *Journal of Physics D: Applied Physics*, 42(6):065202, March 2009.